

Solar energy-driven lignin-first approach to full utilization of lignocellulosic biomass under mild conditions

Xuejiao Wu^{1,2}, Xueting Fan^{1,2}, Shunji Xie^{1,2}, Jinchi Lin¹, Jun Cheng^{1*}, Qinghong Zhang^{1*}, Liangyi Chen¹ and Ye Wang^{1*}

The lignin-first concept offers an opportunity to utilize the entire lignocellulosic biomass efficiently. However, current conversion strategies rely on high-temperature hydrogenolysis by supported metal catalysts, leading to low-functionalized products or difficulty in separation of solid catalyst from cellulose/hemicellulose. Here, we report the fractionation and valorization of lignocellulose via solar energy-driven conversion of native lignin at room temperature. We found that cadmium sulfide quantum dots not only catalyse the cleavage of β -O-4 bonds in lignin models quantitatively but also are efficient for the conversion of native lignin within biomass into functionalized aromatics under visible light, while cellulose/hemicellulose remain almost intact. Further, the colloidal character of quantum dots enables their facile separation and recycling by a reversible aggregation–colloidization strategy. The β -O-4 bond in lignin is cleaved by an electron-hole coupled photoredox mechanism based on a C_α radical intermediate, in which both photogenerated electrons and holes participate in the reaction.

Lignocellulosic biomass, which is composed of lignin, cellulose and hemicellulose, represents more than 90% of all plant biomass and is the largest renewable carbon source without competing with food reserves. Traditional biorefineries have focused on the utilization of the carbohydrate part of lignocellulose with lignin either released as a waste or burnt to generate power (Fig. 1, route A)^{1,2}. To increase the profitability and sustainability of biorefinery, much recent effort has been put into utilizing efficiently all three components of lignocellulose including lignin, which is the most abundant source of renewable aromatics^{2–4}. Although impressive progress has been achieved in the conversion of lignin model compounds and Organosolv lignin into aromatics in recent years^{5–8}, the fractionation of lignocellulose remains challenging^{3,4}. The conventional methods for the fractionation of lignocellulose, such as Kraft and Organosolv processes, usually lead to changes in lignin structure, in particular condensation to form more C–C linkages at the expense of β -O-4 bonds, making the extracted lignin less reactive and more difficult to be transformed⁸.

The lignin-first concept, that is, the catalytic valorization of native lignin in biomass in the first step, offers an opportunity to utilize the entire lignocellulosic biomass in a more efficient manner and has attracted much recent attention^{3,4}. Thus far, hydrogenolysis by a heterogeneous metal catalyst has primarily been employed for the catalytic conversion of native lignin. Often, attention has been paid only to the conversion of lignin, whereas the separation of cellulose/hemicellulose from the solid catalyst remains often neglected (Fig. 1, route B1)^{3,9}. To enable the conversion of entire lignocellulose and the catalyst recycling, multifunctional catalysts, which usually operate under severe reaction conditions, have been exploited to convert both lignin, cellulose and hemicellulose in one pot^{10–12}, but the products are hard to control, and

mixtures of aliphatic alcohols and alkanes are mainly obtained in most cases (Fig. 1, route B2). A few recent studies reported a two-step approach, that is, first valorization of lignin by hydrogenolysis to aromatics under relatively milder conditions and subsequent conversion of cellulose/hemicellulose into aliphatic alcohols or sugar alcohols with the same catalyst under harsher conditions or by adding an acid catalyst (Fig. 1, route B3)^{13,14}. In these cases, the lack of effective contact between the solid catalyst and the solid biomass remains an issue. Thus, a high temperature (typically $\geq 200^\circ\text{C}$) together with a solvent (for example, alcohol) must be used to partially dissolve lignin into small pieces to increase the efficiency of hydrogenolysis^{15,16}. However, the high reaction temperature and high H_2 pressure employed unavoidably led to low-functionalized aromatics, alcohols or alkanes³. These extensively de-functionalized products may require further re-functionalization for high-value chemicals, rendering the process atom inefficient and energy consuming.

In this regard, a method that can activate the dominant linkage in lignin, that is, the β -O-4 ether bond—with a bond dissociation energy (BDE) of $54\text{--}72\text{ kcal mol}^{-1}$ (Fig. 1)¹⁷—under milder conditions and allow for a facile separation of the catalyst from the remaining cellulose/hemicellulose would be ideal. Solar energy-driven catalytic transformations can be utilized for the efficient depolymerization of biomass in a sort of reverse photosynthesis^{18,19}. Some metal complexes and semiconductors have shown promising photocatalytic properties in the cleavage of β -O-4 bond^{20–23}. However, these studies mainly focus on lignin model compounds and use a two-step strategy, that is, first oxidation of $C_\alpha\text{--OH}$ to ketone, which activates the β -O-4 bond, followed by the reductive cleavage of the activated β -O-4 bond. Systems that can use a single photocatalyst for the selective cleavage of β -O-4 bond in one step

¹State Key Laboratory of Physical Chemistry of Solid Surfaces, Collaborative Innovation Center of Chemistry for Energy Materials, National Engineering Laboratory for Green Chemical Productions of Alcohols, Ethers and Esters, College of Chemistry and Chemical Engineering, Xiamen University, Xiamen, China. ²These authors contributed equally to this work: Xuejiao Wu, Xueting Fan, Shunji Xie *e-mail: chengjun@xmu.edu.cn; zhangqh@xmu.edu.cn; wangye@xmu.edu.cn

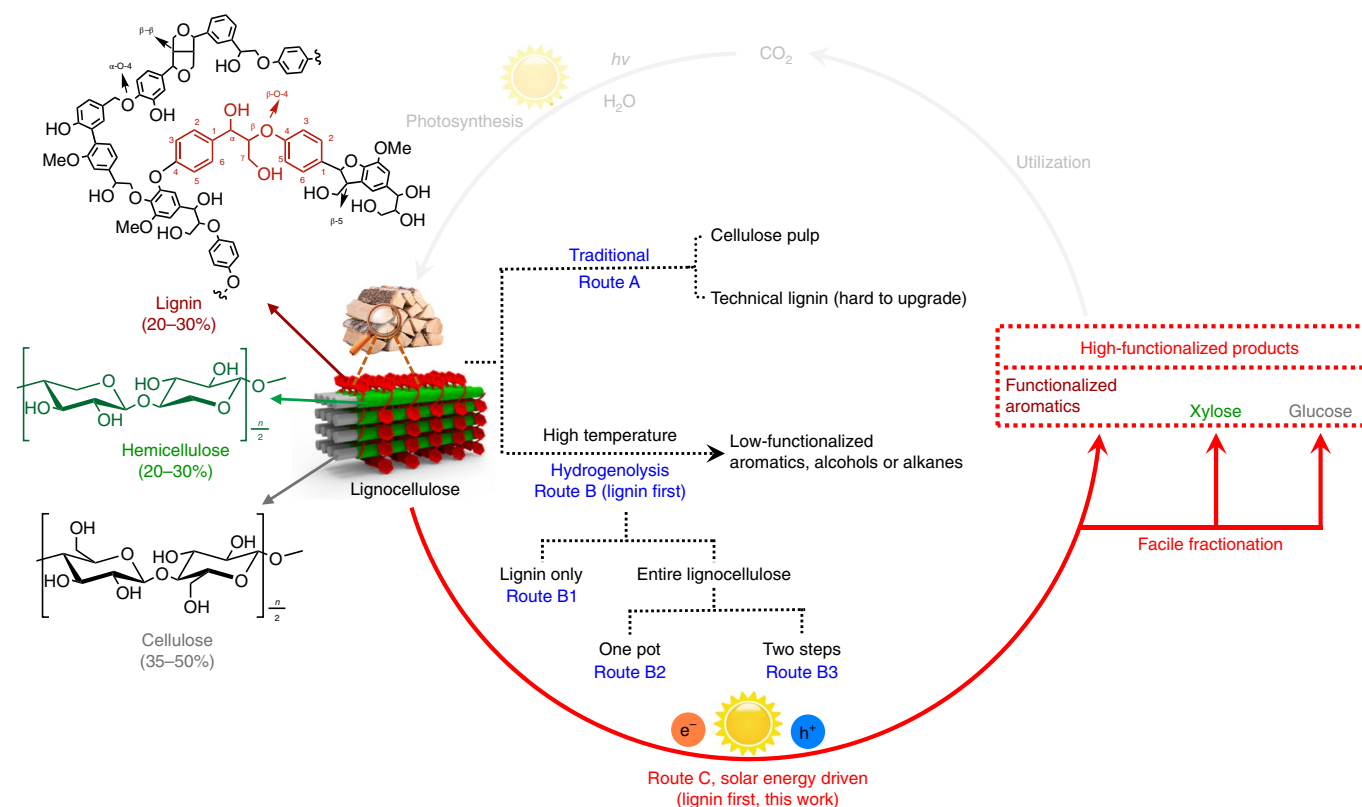


Fig. 1 | Routes for the valorization of lignocellulosic biomass. The β -O-4 linkage is highlighted in the representative lignin fragment. Route A, traditional biorefinery leading to cellulose pulp and technical lignin. Route B, lignin-first approach with high-temperature hydrogenolysis by a supported metal catalyst for the conversion of native lignin. Route C, lignin-first approach with solar energy-driven photocatalytic conversion of lignin under mild conditions.

are rare. Furthermore, no photocatalyst has been reported for the direct conversion of native lignin in solid biomass.

Here, we present an efficient solar energy-driven lignin-first approach for the fractionation and valorization of lignocellulosic biomass into functionalized aromatics, xylose and glucose (Fig. 1, route C). We found that CdS quantum dots (QDs) catalyse the selective cleavage of the β -O-4 bond at room temperature under visible light by an electron-hole coupled (EHCO) mechanism via a C_{α} radical intermediate. The colloidal character of QDs allows intimate contact with the solid biomass substrate, enhancing the accessibility of β -O-4 linkages in biomass by catalyst, and thus enables efficient transformation of native lignin to aromatic monomers under mild conditions. The catalyst can be separated and recycled by a facile aggregation–colloidization strategy.

Results

Performance of CdS QDs for conversion of lignin models. We first performed the photocatalytic conversion of a lignin model compound, 2-phenoxy-1-phenylethanol (PP-ol), at room temperature using some typical semiconductors including TiO_2 , Cu_2O , BiVO_4 , graphitic C_3N_4 , ZnS , CuS and CdS. CdS nanoparticles (NPs) were found to exhibit a very unique performance in breaking the β -O-4 bond under visible light (420–780 nm). CdS NPs with cubic zinc blende structure and diameters of 20–40 nm (Supplementary Fig. 1) showed significantly higher activity than other semiconductors in Fig. 2a. Compared with some typical thermocatalytic systems with PP-ol as the substrate, the present CdS-catalysed photocatalytic system also exhibited a higher activity or product selectivity under mild conditions (Supplementary Table 1). Different from most of the previous catalytic systems, our system is highly selective for the cleavage of the β -O-4 bond, producing acetophenone and phenol almost in stoichiometric amounts.

Semiconductor nanocrystals with sizes smaller than the Bohr exciton diameter are known as QDs due to the quantum confinement effects, which can increase the energy of excitons and enhance the photocatalytic performance^{24,25}. We synthesized CdS QDs (size <6.4 nm) with mean sizes varying from 3.8 to 6.1 nm (Supplementary Fig. 1) and confirmed the increases in bandgap and redox capability of photogenerated electrons and holes for the QDs (Supplementary Fig. 1e,f and Fig. 2b)^{24,26}. The activity of CdS QDs for the conversion of PP-ol was significantly higher than that of CdS NPs, and high yields of acetophenone and phenol could be obtained even in 3 h of reaction (Fig. 2b). The CdS QDs with a size of 4.4 nm (denoted as CdS QD–4.4 nm) showed the highest product yields (>90%). The rate of PP-ol conversion for CdS QD–4.4 nm was approximately four times higher than that of CdS NPs. Further studies were performed to understand the size effect of CdS QDs. First, we showed that the surface area plays a key role in photocatalytic conversion of PP-ol. The increase in the surface area by increasing the amount of the CdS QD–4.4 nm catalyst enhanced the conversion (Supplementary Fig. 2a). Then, we compared the activity per surface area for CdS QDs with different sizes. A 395 nm LED light was employed to eliminate the influence of light absorption. Actually, we observed a decrease in activity with a decrease in the size of CdS QDs from 4.4 to 3.8 nm under the irradiation of Xe lamp (wavelength λ = 420–780 nm) (Fig. 2b), and this probably arose from the poor light absorption of the CdS QDs–3.8 nm in the visible light range due to the increase in bandgap. Under the irradiation with the 395 nm LED light, the rate of PP-ol conversion per surface area increased significantly on decreasing the size of CdS QDs (Supplementary Fig. 2b). Thus, the higher redox capability of photogenerated excitons also contributes to the higher photocatalytic activity of smaller CdS QDs.

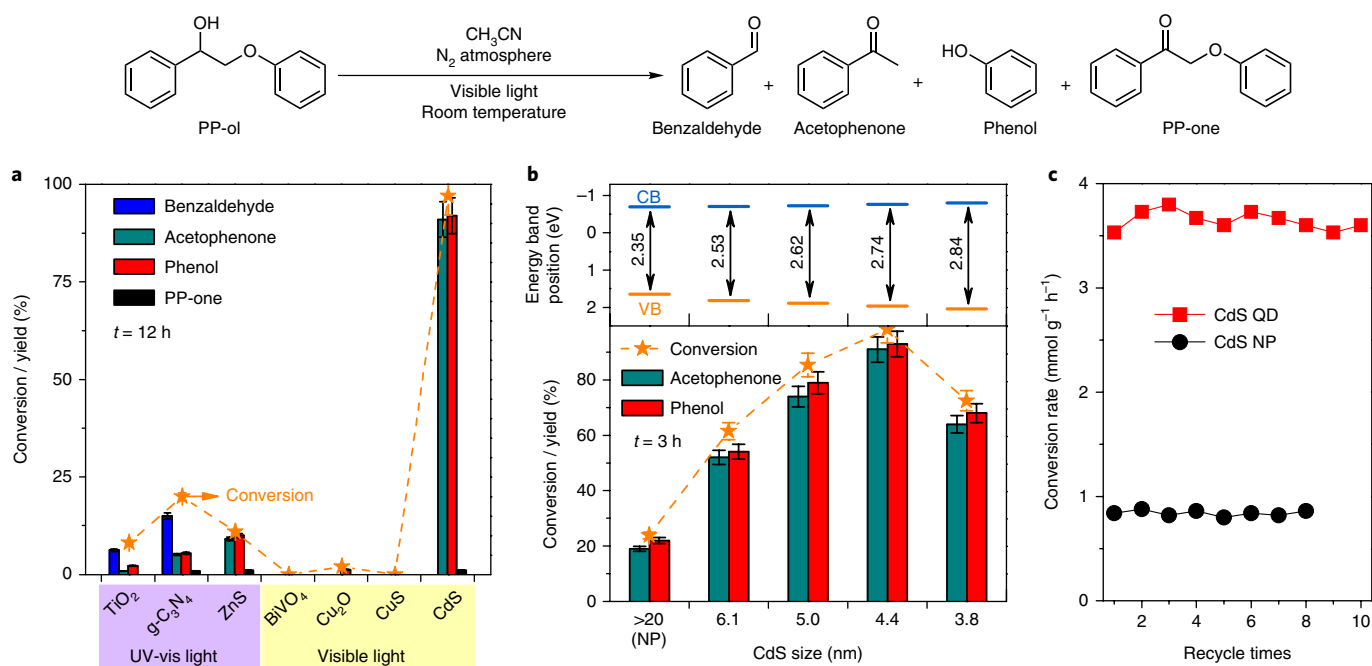


Fig. 2 | Photocatalytic cleavage of β -O-4 bond in lignin model compounds. **a**, Photocatalytic conversion of PP-ol with several typical semiconductors. **b**, Energy-band positions and photocatalytic performances of CdS with different sizes. **c**, Repeated uses of CdS NPs and CdS QD–4.4 nm for the conversion of PP-ol. The reaction was carried out under visible light irradiation ($\lambda = 420\text{--}780\text{ nm}$). The UV-visible light ($\lambda = 300\text{--}780\text{ nm}$) irradiation was applied to several semiconductors in Fig. 2a. The experiments in each case were performed at least three times. The error bars represent the relative deviation, which is within 5%. The curves in each figure are guides to the eye.

Our control experiments for the CdS QD–4.4 nm-catalysed PP-ol conversion with different solvents did not show significant differences in catalytic performances, indicating that CdS QDs are tolerant of various environments (Supplementary Table 2). CdS QDs as well as CdS NPs were stable during the reaction, as shown by inductively coupled plasma mass spectrometry analysis of the post-reaction mixture after catalyst removal, which confirmed the absence of cadmium in solution. In addition, no deactivation was observed for the CdS QD–4.4 nm after 10 recycling experiments (Fig. 2c and Supplementary Fig. 3).

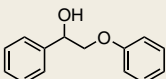
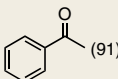
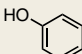
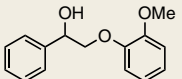
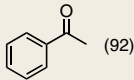
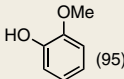
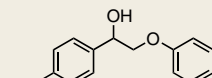
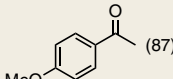
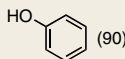
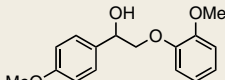
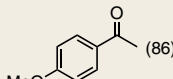
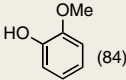
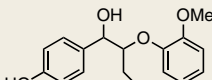
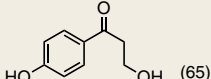
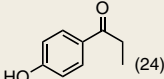
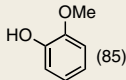
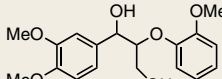
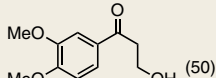
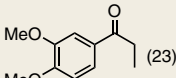
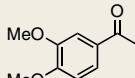
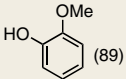
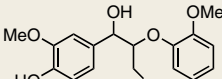
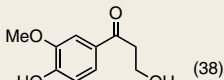
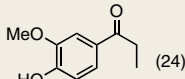
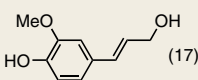
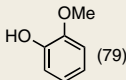
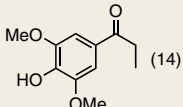
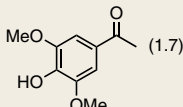
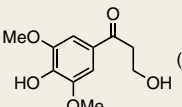
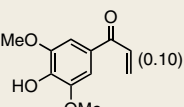
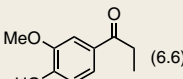
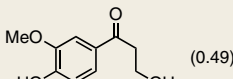
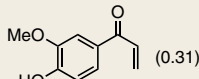
Furthermore, the CdS QD–4.4 nm could efficiently catalyse the cleavage of the β -O-4 bond in a wide range of lignin model compounds, and the functional groups such as phenol, ketone and methoxy groups remained almost intact (Table 1). The γ -hydroxyl group, which could easily undergo degradation, was also partially retained.

Native lignin conversion by soluble colloidal CdS QDs. Compared with lignin model compounds, the conversion of native lignin is much more difficult. Lignin is intertwined with carbohydrates in lignocellulose, limiting the access of the catalytic active site to the targeted linkage. Homogeneous catalysts are capable of penetrating better to specific linkages and may be promising for the valorization of lignocellulose²⁷, but they still face problem of separation with liquid products²⁸. Moreover, although many homogeneous catalysts have been reported for the conversion of lignin model compounds, few show considerable activity for the depolymerization of native lignin^{5–8,27}. To overcome the low efficiency of solid–solid contact between heterogeneous catalyst and solid biomass, high-temperature solvolysis of lignin has been adopted in most heterogeneous catalytic systems (Fig. 3a)^{3,4}. Here, we propose a solubilizing catalyst method instead of solubilizing lignin (Fig. 3a). QDs with surface organic surfactants are of colloidal nature and can be highly dispersed or solubilized in proper solvents by tuning the organic

ligand²⁹. This enables the implementation of the solubilizing catalyst method. A hydrophilic ligand, 3-mercaptopropionic acid (MPA), is typically used in the present work and makes CdS QDs highly dispersed or soluble in aqueous solution.

The CdS QDs with MPA ligand (denoted as CdS–MPA) have been used for photocatalytic conversion of native lignin in birch woodmeal at room temperature under visible light ($\lambda = 400\text{--}780\text{ nm}$). The contents of monomeric units and the percentage of β -O-4 linkages in the native biomass were characterized by two-dimensional heteronuclear single quantum coherence NMR (2D HSQC NMR) (Supplementary Fig. 4 and Supplementary Table 3). The theoretical maximum yield of aromatic monomers by assuming the selective cleavage of β -O-4 linkages was calculated to be 32 wt% (see Methods and Supplementary Table 4). We have devised a reversible aggregation–colloidization strategy for the separation and recycling of CdS QD catalyst. After photocatalysis, the CdS–MPA was aggregated or insolubilized by adding an organic solvent, acetone, and was separated with the liquid products. The major products in liquid phase were functionalized aromatic monomers, in particular syringyl- and guaiacyl-derived ketones (denoted as S-ketones and G-ketones) (Supplementary Figs. 5 and 6). These products are analogues to those observed in the conversion of model compounds with γ -C–OH group (Table 1, entries 5–7). We propose that S- and G-ketones are formed via the cleavage of β -O-4 bonds and the vulnerability of the γ tail results in ketones with different side chains (Supplementary Table 5). The ratio of products belonging to S and G units in the products was evaluated to be 2.4, which was almost identical to that in the original lignin characterized by 2D HSQC NMR (2.3). The total yield of monomeric aromatics was 26.7 wt% (Fig. 3b). This yield corresponds to 84% of the theoretical maximum evaluated by the 2D HSQC NMR. The aromatic components in biomass are not only connected with each other through different linkages but also are partially bonded to polysaccharides (known as lignin–carbohydrate complex)³⁰,

Table 1 | Products from photocatalytic conversions of lignin models and birch woodmeal

Entry no.	Reactant	Time (h)	Conversion (%)	Yield (%)			
1		3	99	 (91)	 (93)		
2		4	99	 (92)	 (95)		
3		4	99	 (87)	 (90)		
4		8	92	 (86)	 (84)		
5		12	94	 (65)	 (24)	 (85)	
6		12	95	 (50)	 (23)	 (8.2)	 (89)
7		20	89	 (38)	 (24)	 (17)	 (79)
S-ketone							
8	Birch woodmeal ^a	8		 (14)	 (1.7)	 (1.5)	 (0.10)
G-ketone							
				 (6.6)	 (0.49)	 (0.31)	

^aSee Supplementary Table 5 for other products.

leading to difficulty in obtaining 100% of the theoretical maximum. It is noteworthy that the functional groups in our products remain almost intact because of the mild conditions used. Furthermore, the reaction was successfully scaled-up, and the major product, 1-(3,5-dimethoxy-4-hydroxyphenyl)-1-propanone, was isolated with a 10.6 wt% (24 mg) yield, close to the yield (12 wt%) determined by gas chromatograph (GC) (see Supplementary Table 5 and Supplementary Methods).

The aggregated CdS QDs could be re-colloidized or re-dispersed in aqueous solution and could be facily separated from the solid cellulose/hemicellulose residue. The repeated uses of the catalyst by the reversible aggregation–colloidization strategy demonstrated that the yield of aromatic monomers did not decrease significantly (Fig. 3c).

Our control experiments showed that no product was formed in the absence of a catalyst or without light irradiation. Moreover,

the particulate CdS, which catalysed the conversion of lignin model compounds (Fig. 2), only showed a very low activity in the conversion of native lignin (product yield = 1.2%) (Fig. 3b and Supplementary Table 6). We also found that the change of surface ligand of CdS QDs from MPA to 1-mercaptopropane, which caused the aggregation of QDs in aqueous solution, significantly decreased the product yield from 26.7 to 4.9% (Fig. 3b). Furthermore, ZnIn₂S₄, a recently reported photocatalyst efficient for the cleavage of β-O-4 bonds in lignin model compounds and extracts²³, exhibited a markedly lower yield (1.9%) of aromatic monomers in native lignin transformation (Supplementary Table 6). These results clearly demonstrate the effectiveness of the solubilizing catalyst method in the conversion of native lignin to realize the lignin-first concept for biomass utilization under mild conditions.

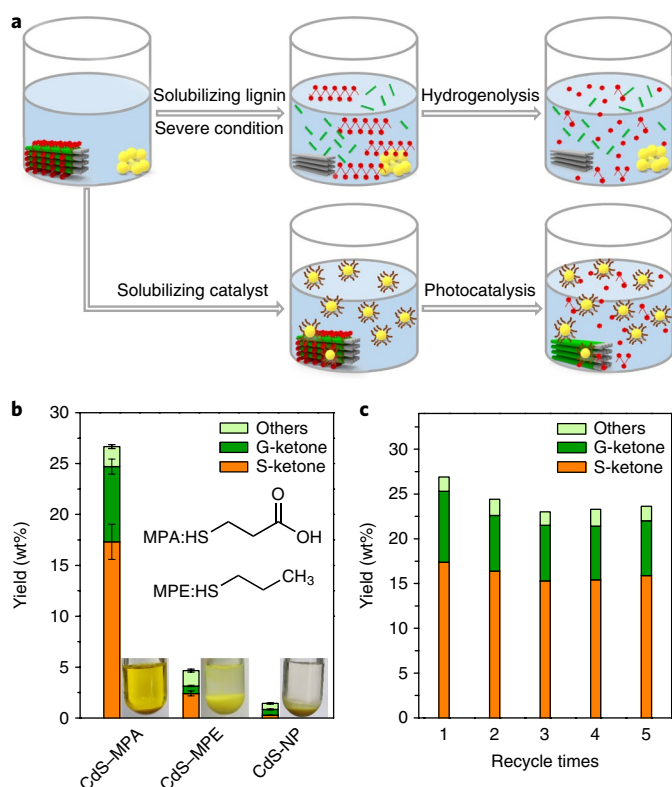


Fig. 3 | Photocatalytic conversion of native lignin in birch woodmeal.

a, Schematic of solubilizing catalyst method by high-dispersion colloidal CdS QDs compared with the traditional solubilizing lignin method by high-temperature hydrogenolysis. The red line, sphere and structure represent lignin; the yellow sphere represents CdS QD; the green stick represents hemicellulose; the grey structure represents cellulose; the brown line represents ligand. **b**, Yield of aromatic monomers obtained with different photocatalysts. Inset images: mixture of birch woodmeal with different catalysts. MPE, 1-mercaptopropane. **c**, Repeated uses of CdS-MPA QDs. The experiments in each case were performed at least three times. The error bars represent the relative deviation, which is within 10%.

Full utilization of entire lignocellulose. The lignin-first concept would become more viable if cellulose/hemicellulose components can survive after lignin transformation and can be incorporated into the current biorefinery system. Our method for the valorization of entire lignocellulose is schematically displayed in Fig. 4a. We have measured the compositions of the solid residue (see Supplementary Methods) after photocatalytic conversion of native lignin in birch woodmeal and catalyst separation by re-colloidization. The contents of xylans and glucans were 18wt% and 43wt% (Fig. 4b), respectively, corresponding to 90% and 98% of those in the original birch woodmeal (Supplementary Table 7). This indicates that hemicellulose and cellulose remain almost intact. It is worth pointing out that the preservation of hemicellulose is a particularly challenging but alluring task in the lignocellulose fractionation process because hemicellulose easily undergoes degradation in the conventional high-temperature biorefinery or lignin-first fractionation by hydrogenolysis⁴. Our control experiments using cellulose, hemicellulose, glucose and xylose as substrates confirmed that they could be kept under our photocatalytic conditions. Therefore, our solar energy-driven conversion of native lignin at room temperature provides a promising approach to retaining hemicellulose and cellulose.

We have performed catalytic transformations of the solid residue containing hemicellulose and cellulose. After separation with the re-colloidized CdS QDs, the solid residue (fraction I) was

first subjected to acidolysis under mild conditions (see Methods). Xylose with a yield of 84% was obtained (Fig. 4c and Supplementary Fig. 8). Then, an enzymatic hydrolysis was performed for the remaining solid (fraction II). Glucose with a yield of 91% was obtained (Fig. 4c and Supplementary Fig. 8). To the best of our knowledge, this is first example to demonstrate that the lignin-first fractionation of lignocellulose could be integrated with the current biorefinery system without compromising carbohydrate fractions.

Mechanism for β -O-4 bond cleavage. The efficient cleavage of β -O-4 linkages in native lignin is the core of the present approach. We have performed mechanistic studies to understand the chemistry of the solar energy-driven cleavage of β -O-4 bond at room temperature. The photocatalytic conversion of 2-phenoxy-1-phenylethanone (PP-one) with or without CH₃OH (as a hydrogen donor) was very slow in the presence of CdS QD-4.4nm catalyst (Fig. 5a (i) and (ii)). This finding is different from the previous studies on photocatalytic^{20–23} or non-photocatalytic systems^{31–33}, which have pointed out that the cleavage of β -O-4 bond proceeds via pre-oxidation of C _{α} -OH to C _{α} =O. Thus, our system may differ from the previous two-step photocatalytic systems in mechanism^{20–23}. The control experiments using electron and hole scavengers showed significantly decreased performances for the conversion of PP-ol (Fig. 5a (iii)–(v)), indicating that both photogenerated electrons and holes participated in the formation of acetophenone and phenol. We believe that the full use of both electrons and holes in PP-ol conversion leads to high stability of CdS in the absence of any sacrificial reagent (Figs. 2c and 3c). The addition of small amount of 5,5-dimethyl-1-pyrroline-N-oxide (DMPO), a radical scavenger, also suppressed the reaction (Fig. 5a (vi)), suggesting that the reaction proceeded via radical intermediates. Furthermore, the reaction completely stopped when the benzylic hydrogen was replaced by a methyl group (Fig. 5a (vii)). Thus, the presence of C _{α} hydrogen is crucial to the reaction.

Density functional theory (DFT) calculations were performed to gain insights into reaction intermediates and pathways. We calculated the adsorption of PP-ol and three possible radical intermediates, formed by cleaving the C _{α} -H, C _{β} -H and O-H bonds, on CdS surfaces, and found that the C _{α} radical is the most stable intermediate (Supplementary Fig. 9 and Supplementary Table 9). We converted the calculated energies into the potentials versus standard hydrogen electrode (SHE) for the oxidative dehydrogenation (ODH) of PP-ol to radical intermediates^{34–36}, so that they could be compared against the energy-band positions of CdS. As shown in Fig. 5b, the C _{α} -H bond cleavage has the least positive ODH potential (1.1 V versus SHE), indicating that the C _{α} -H bond will first break on oxidation by holes. Moreover, the valence band maximum (VBM) of CdS (1.7 V versus SHE) is more positive than the C _{α} -H bond ODH potential. Thus, the photoexcited hole can sufficiently oxidize PP-ol into the C _{α} radical. Our calculation also confirms the experimental finding that the C _{α} hydrogen plays a critical role in the reaction.

The formation of C _{α} radical has been verified by a powerful spin trap, 5-diisopropoxy-phosphoryl-5-methyl-1-pyrroline-N-oxide (DIPPMPO). Generally, DIPPMPO can react with free radicals to form nitroxide intermediate, which undergoes disproportionation to produce corresponding stable hydroxylamine and nitron as final products (Fig. 5c)^{37,38}. The positive-ion electrospray ionization mass spectrum of the product mixture after the addition of DIPPMPO unequivocally confirmed the presence of C _{α} radical (Fig. 5d); the major mass peak (478.2) could be assigned to C _{α} radical-induced hydroxylamine ($m + 1 = 478$). The ³¹P NMR spectrum demonstrated a dominated signal at 28.7 ppm (Fig. 5e), which corresponded to C _{α} radical adducts³⁸. This provides further evidence for the formation of the C _{α} radical as the reaction intermediate in our system.

We further studied the subsequent cleavage of β -O-4 bond in the C _{α} radical. The ODH of PP-ol to the C _{α} radical markedly decreases the BDE of the β -O-4 bond from 55 to 7.8 kcal mol⁻¹ (Fig. 5f and

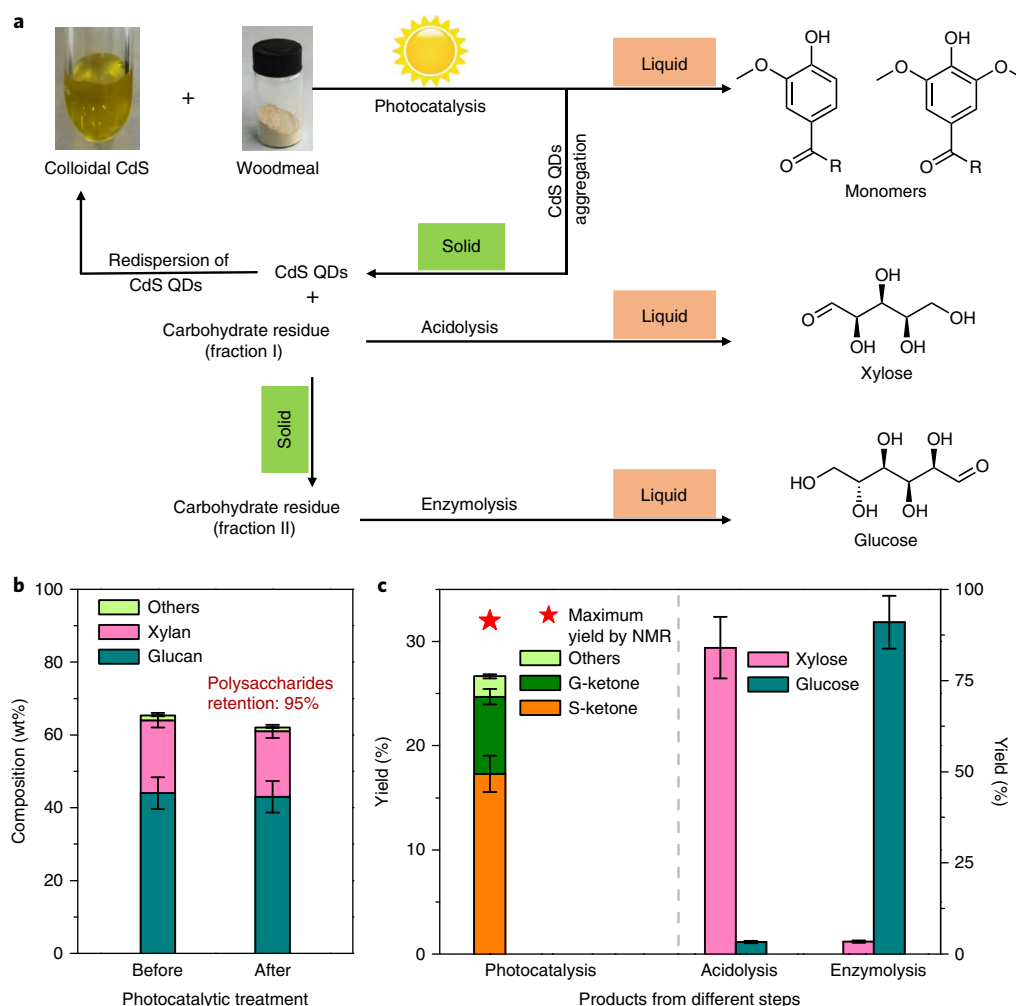


Fig. 4 | Valorization of entire lignocellulosic biomass. **a**, Schematic of the whole process for solar energy-driven lignin-first valorization of birch woodmeal. **b**, Compositions of xylans and glucans in birch woodmeal before and after photocatalytic conversion. **c**, Yields of products obtained in photocatalysis, acidolysis and enzymolysis. The experiments in each case were performed at least three times. The error bars represent the relative deviation, which is within 10%.

Supplementary Fig. 10). Such a decrease is significantly larger than that by oxidizing the C_{α} -OH to C_{α} =O, where the BDE of the β -O-4 bond decreases from 55 to 47 kcal mol⁻¹. We believe that the remarkably lower BDE of the β -O-4 bond in the C_{α} radical intermediate is the key reason for the high activity and selectivity of our system. The cleavage of the β -O-4 bond in the C_{α} radical, which produces acetophenone and phenoxy radical, is also much easier than the cleavage of the C_{α} -C $_{\beta}$ and the O-H bonds (Supplementary Fig. 10).

The C_{α} radical has been reported as an intermediate in the degradation of lignin, leading to undesirable photoyellowing of paper^{39,40}. Several studies have reported that the C_{α} radical can be generated by photolysis and the generation can be accelerated in the presence of hydrogen-atom abstracting species³⁹. However, the photocatalytic cleavage of β -O-4 bond through C_{α} radical intermediate remains undiscovered to date. Through DFT calculation, we clarified that when accepting an electron, the C_{α} radical underwent facile β -O-4 bond breaking, spontaneously forming acetophenone and phenoxy anion during geometry optimization. The calculated reduction potential of this process is -0.21 V versus SHE (Supplementary Fig. 10), lower than the conduction band minimum (CBM) of CdS (Fig. 5b), indicating that the photogenerated electron can readily drive the reductive cleavage of β -O-4 bond in the C_{α} radical. Therefore, our experimental

and computational results both reveal an EHCO mechanism, in which the C_{α} radical intermediate is first formed via the ODH of the C_{α} -H bond driven by the hole, and then the intermediate undertakes a reductive cleavage of the β -O-4 bond triggered by the electron.

Conclusions

We have found that CdS QDs are powerful catalysts for the selective cleavage of the β -O-4 bond in various lignin model compounds at room temperature under visible light. The functional groups remain almost intact during the breaking of the β -O-4 bond. The colloidal character of CdS QDs enables intimate contact between soluble catalyst and solid lignocellulosic biomass, thus making the present photocatalytic system highly efficient for the conversion of native lignin in solid biomass at room temperature. Functionalized aromatic monomers, mainly ketones, are obtained with a yield of about 27 wt% from birch woodmeal, corresponding to 84% of the theoretical maximum by assuming the selective cleavage of β -O-4 linkages. The hemicellulose and cellulose can survive after the photocatalytic transformation of lignin. We have developed an aggregation-colloidization strategy for separation of catalyst from aromatic products and the remaining solid cellulose/hemicellulose residue. Xylose and glucose are obtained from the solid residue with yields of 84% and 91% by acidolysis and enzymolysis, respectively.

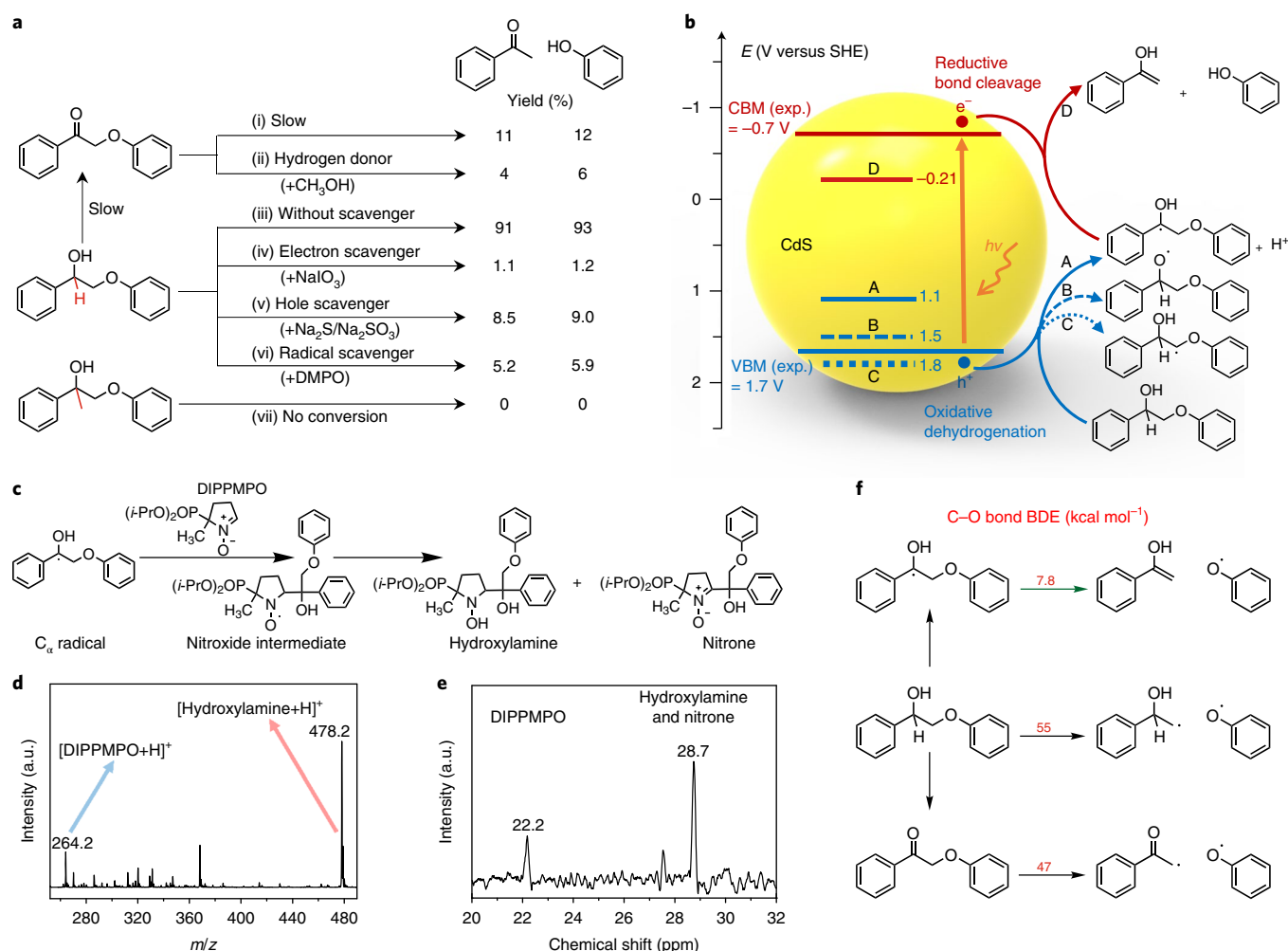


Fig. 5 | Mechanism for solar energy-driven cleavage of β -O-4 bond. **a**, Control experiments with different reactants or additives catalysed by CdS QD—4.4 nm under visible light. Hydrogen donor in PP-one control reaction, CH₃OH 0.5 ml. Scavenger concentrations: 2.0 mM NaIO₃; 4.0 mM Na₂S + 2.0 mM Na₂SO₃; 3.0 mM DMPO. Reaction time: 3 h. **b**, Potentials of oxidative dehydrogenation of PP-ol via three different paths (A, B, C) and potential of reductive cleavage of β -O-4 bond in the C _{α} radical intermediate (D) against the positions of VBM and CBM of CdS. Experimental values of VBM and CBM were obtained through UV-visible and electrochemical measurements of bulk CdS (Supplementary Fig. 1). **c**, Spin trapping reaction of C _{α} radical with DIPPMPPO. **d**, Positive-ion electrospray ionization mass spectrum. **e**, ³¹P NMR spectrum of product mixture. The reaction was performed under standard conditions except for adding 10 mM DIPPMPPO. **f**, Comparison of BDE of β -O-4 bond in C _{α} radical with those in PP-ol and PP-one.

Our mechanistic studies reveal that the cleavage of the β -O-4 bond proceeds through a photoredox EHCO mechanism, in which both photogenerated electrons and holes participate in the formation of products. The C _{α} radical, which is formed as an intermediate during the photochemical process, possesses a β -O-4 bond with a markedly decreased BDE. Thus, the present photoredox process is very specific towards the cleavage of β -O-4 linkages. The present work not only offers a promising tool to cleave precisely the β -O-4 bond but also opens an avenue for the full utilization of lignocellulosic biomass by the lignin-first approach under mild conditions.

Methods

Evaluation of photocatalytic performance. For the conversion of lignin model compounds, typically 5 ml CH₃CN, 10 mg catalyst and 0.1 mmol lignin model compound (~20 mg) were added into a quartz reactor (10 ml). The reactor was evacuated and purged with N₂ for several minutes. The reaction mixture was stirred at 1,000 r.p.m. and underwent reaction under visible light irradiation. The light source was a 300 W Xe lamp with an ultraviolet (UV) cut-off filter ($\lambda \geq 420$ nm). The UV-visible light irradiation without using the UV cut-off filter was also applied to some catalysts. The reaction was typically carried out for 12 h for CdS NPs and 3 h for CdS QDs. After reaction, the mixture was centrifuged at

9,000 r.p.m. (9,056g) for 5 min and the catalyst was recovered by filtration. The products were quantified by high-performance liquid chromatography (HPLC). In some cases, GC-mass spectrometry (GC-MS) and GC with flame ionization detector (GC-FID) were also used for product identification and quantification.

For the photocatalytic conversion of native lignin, typically 15 mg catalyst and 100 mg birch woodmeal were added into the quartz reactor (10 ml). The reaction conditions were basically the same as those for the conversion of lignin model compounds except for using CH₃OH/H₂O (5 ml) as the solvent and a reaction time of 8 h. The light source used for the conversion of native lignin was a 300 W Xe lamp with a UV cut-off filter ($\lambda \geq 400$ nm).

Quantification of aromatic monomers from native lignin. After photocatalytic reaction, an internal standard solution (50 μ l), 400 mg methyl 4-hydroxybenzoate in 100 ml acetone, was added to the product mixture for quantification. Adequate amount of acetone (typically 20 ml) was added into the reaction solution to allow the aggregation of CdS QDs modified by MPA ligand. The mixture was centrifuged, and the aggregated catalyst and cellulose/hemicellulose residue were collected by filtration. The filtrate was concentrated to about 2 ml, and then the products in the filtrate were identified by GC-MS and quantified by GC-FID. The following operation conditions were used for GC-FID: injection temperature, 280 °C; column temperature programme: 50 °C for 3 min, then increasing the temperature to 290 °C at a rate of 10 °C per min, then holding at 290 °C for 10 min; detection temperature, 290 °C. Effective carbon number method was used for

quantification⁴¹. The effective carbon numbers of our products are shown in Supplementary Table 8.

Calculation of theoretical maximum aromatic monomer yield. The maximum yield of aromatic monomers is lower than the fraction of β -O-4 linkages in native lignin. This is because a monomer can only be released when it is flanked by two β -O-4 bonds. The 2D HSQC NMR spectra were acquired by a method reported previously to evaluate the abundances of monomers and linkages in native lignin⁴². The assignments (Supplementary Table 3) are consistent with those reported previously⁴³.

Theoretical maximum monomer yield was calculated by the following equation^{3,32}:

$$\text{Maximum monomer yield} \approx P'(\beta\text{-O-4}) \times P'(\beta\text{-O-4}) \quad (1)$$

where $P'(\beta\text{-O-4})$, which is the probability of releasable β -O-4 bonds, is obtained using the following equation:

$$P'(\beta\text{-O-4}) = P(\beta\text{-O-4}) \times [1 - P(\text{S condensed})] \quad (2)$$

where $P(\beta\text{-O-4})$ represents the number of β -O-4 linkages per 100 C_9 units and $P(\text{S condensed})$ represents the number of condensed syringyl (S) monomers per 100 C_9 units. Both values could be obtained from the 2D HSQC NMR integration results (see Supplementary Table 4 for details).

Acidolysis and enzymolysis of hemicellulose/cellulose. After separation of catalyst by re-colloidization, the solid hemicellulose/cellulose residue (fraction I) was rinsed thoroughly (3×4 ml) with a 2 wt% H_2SO_4 solution and was placed in a 50 ml beaker. H_2SO_4 solution (2 wt%) was further added to the beaker to make the final liquid volume 20 ml, and the mixture was kept at 100 °C for 2 h under stirring. The resultant liquid was used for HPLC analysis to quantify the product.

After acidolysis, the solid residue (fraction II) was recovered by centrifugation and was rinsed thoroughly (3×4 ml) with 0.1 mol l^{-1} acetate buffer (pH = 4.5). Then, the solid residue was placed in a 50 ml beaker. Acetate buffer was added to the beaker to make the final liquid volume 20 ml. Cellulase (cellulase from *Trichoderma reesei*, Sigma, 30 FPU (filter paper units) per g glucan) was added into the beaker, followed by stirring at 37 °C. The resultant liquid was used for HPLC analysis to quantify the product¹⁶.

DFT calculations. The adsorption of PP-ol and relevant surface intermediates on the CdS(110) surface were calculated using the freely available program package CP2K/Quickstep⁴⁴. The gradient-corrected Perdew–Burke–Ernzerhof (GGA-PBE) functional⁴⁵ and hybrid HSE06⁴⁶ were used with the Grimme's dispersion correction⁴⁷. The bond dissociation energies of the C_p –O bonds and redox potentials of PP-ol and intermediates were also calculated using the Gaussian 09 program package⁴⁸, in which hybrid B3LYP⁴⁹ and C-PCM⁵⁰ implicit solvation model were used. More details on computational setup can be found in the Supplementary Information.

The experimental details for the analyses of substrates and products, the characterizations of catalysts, the syntheses of CdS NPs and QDs, ligand exchange procedure and method of biomass compositional analysis are described in Supplementary Methods. The computational details including the models of CdS surfaces, the computational setup, the calculations of oxidative dehydrogenation of PP-ol, BDEs and redox potentials are also displayed in Supplementary Methods.

Data availability

The data supporting the findings of this study are available from the corresponding authors upon reasonable request.

Received: 16 August 2017; Accepted: 17 August 2018;

Published online: 01 October 2018

References

- Tuck, C. O., Pérez, E., Horváth, I. T., Sheldon, R. A. & Poliakoff, M. Valorization of biomass: deriving more value from waste. *Science* **337**, 695–699 (2012).
- Ragauskas, A. J. et al. Lignin valorization: improving lignin processing in the biorefinery. *Science* **344**, 1246843 (2014).
- Galkin, M. V. & Samec, J. S. Lignin valorization through catalytic lignocellulose fractionation: a fundamental platform for the future biorefinery. *ChemSusChem* **9**, 1544–1558 (2016).
- Renders, T., Van den Bosch, S., Koelewijn, S. F., Schutyser, W. & Sels, B. F. Lignin-first biomass fractionation: the advent of active stabilisation strategies. *Energy Environ. Sci.* **10**, 1551–1557 (2017).
- Zakzeski, J., Bruijninx, P. C. A., Jongerius, A. L. & Weckhuysen, B. M. The catalytic valorization of lignin for the production of renewable chemicals. *Chem. Rev.* **110**, 3552–3599 (2010).
- Xu, C., Arancon, R. A. D., Labidi, J. & Luque, R. Lignin depolymerisation strategies: towards valuable chemicals and fuels. *Chem. Soc. Rev.* **43**, 7485–7500 (2014).
- Li, C., Zhao, X., Wang, A., Huber, G. W. & Zhang, T. Catalytic transformation of lignin for the production of chemicals and fuels. *Chem. Rev.* **115**, 11559–11624 (2015).
- Rinaldi, R. et al. Paving the way for lignin valorisation: recent advances in bioengineering, biorefining and catalysis. *Angew. Chem. Int. Ed.* **55**, 8164–8215 (2016).
- Yan, N. et al. Selective degradation of wood lignin over noble-metal catalysts in a two-step process. *ChemSusChem* **1**, 626–629 (2008).
- Matson, T. D., Barta, K., Iretskii, A. V. & Ford, P. C. One-pot catalytic conversion of cellulose and of woody biomass solids to liquid fuels. *J. Am. Chem. Soc.* **133**, 14090–14097 (2011).
- Li, C., Zheng, M., Wang, A. & Zhang, T. One-pot catalytic hydrocracking of raw woody biomass into chemicals over supported carbide catalysts: simultaneous conversion of cellulose, hemicellulose and lignin. *Energy Environ. Sci.* **5**, 6383–6390 (2012).
- Xia, Q. et al. Direct hydrodeoxygenation of raw woody biomass into liquid alkanes. *Nat. Commun.* **7**, 11162 (2016).
- Van den Bosch, S. et al. Reductive lignocellulose fractionation into soluble lignin-derived phenolic monomers and dimers and processable carbohydrate pulps. *Energy Environ. Sci.* **8**, 1748–1763 (2015).
- Sun, Z. et al. Complete lignocellulose conversion with integrated catalyst recycling yielding valuable aromatics and fuels. *Nat. Catal.* **1**, 82–92 (2018).
- Song, Q. et al. Lignin depolymerization (LDP) in alcohol over nickel-based catalysts via a fragmentation–hydrogenolysis process. *Energy Environ. Sci.* **6**, 994–1007 (2013).
- Ferrini, P. & Rinaldi, R. Catalytic biorefining of plant biomass to non-pyrolytic lignin bio-oil and carbohydrates through hydrogen transfer reactions. *Angew. Chem. Int. Ed.* **53**, 8634–8639 (2014).
- Kim, S. et al. Computational study of bond dissociation enthalpies for a large range of native and modified lignins. *J. Phys. Chem. Lett.* **2**, 2846–2852 (2001).
- Lanzalunga, O. & Bietti, M. Photo- and radiation chemical induced degradation of lignin model compounds. *J. Photochem. Photobiol. B* **56**, 85–108 (2000).
- Li, S. H., Liu, S., Colmenares, J. C. & Xu, Y. J. A sustainable approach for lignin valorization by heterogeneous photocatalysis. *Green. Chem.* **18**, 594–607 (2016).
- Nguyen, J. D., Matsuura, B. S. & Stephenson, C. R. J. A photochemical strategy for lignin degradation at room temperature. *J. Am. Chem. Soc.* **136**, 1218–1221 (2014).
- Bosque, I. et al. Redox catalysis facilitates lignin depolymerization. *ACS Cent. Sci.* **3**, 249–621 (2017).
- Luo, N. et al. Photocatalytic oxidation–hydrogenolysis of lignin β -O-4 models via a dual light wavelength switching strategy. *ACS Catal.* **6**, 7716–7721 (2016).
- Luo, N. et al. Visible-light-driven self-hydrogen transfer hydrogenolysis of lignin models and extracts into phenolic products. *ACS Catal.* **7**, 4571–4580 (2017).
- Zhao, J., Holmes, M. A. & Osterloh, F. E. Quantum confinement controls photocatalysis: a free energy analysis for photocatalytic proton reduction at CdSe nanocrystals. *ACS Nano* **7**, 4316–4325 (2013).
- Zhao, L. M. et al. Photocatalysis with quantum dots and visible light: selective and efficient oxidation of alcohols to carbonyl compounds through a radical relay process in water. *Angew. Chem. Int. Ed.* **56**, 3020–3024 (2017).
- Simon, T. et al. Redox shuttle mechanism enhances photocatalytic H_2 generation on Ni-decorated CdS nanorods. *Nat. Mater.* **13**, 1013–1018 (2014).
- Deuss, P. J., Barta, K. & de Vries, J. G. Homogeneous catalysis for the conversion of biomass and biomass-derived platform chemicals. *Catal. Sci. Technol.* **4**, 1174–1196 (2014).
- Rinaldi, R. & Schüth, F. Design of solid catalysts for the conversion of biomass. *Energy Environ. Sci.* **2**, 610–626 (2009).
- Boles, M. A., Ling, D., Hyeon, T. & Talapin, D. V. The surface science of nanocrystals. *Nat. Mater.* **15**, 141–153 (2016).
- Yuan, T. Q., Sun, S. N., Xu, F. & Sun, R. C. Characterization of lignin structures and lignin–carbohydrate complex (LCC) linkages by quantitative ^{13}C and 2D HSQC NMR spectroscopy. *J. Agric. Food Chem.* **59**, 10604–10614 (2011).
- Rahimi, A., Ulbrich, A., Coon, J. J. & Stahl, S. S. Formic-acid-induced depolymerization of oxidized lignin to aromatics. *Nature* **515**, 249–252 (2014).
- Lancefield, C. S., Ojo, O. S., Tran, F. & Westwood, N. J. Isolation of functionalized phenolic monomers through selective oxidation and C–O bond cleavage of the β -O-4 linkages in lignin. *Angew. Chem. Int. Ed.* **54**, 258–262 (2015).
- Deng, W. et al. Oxidative conversion of lignin and lignin model compounds catalyzed by CeO_2 -supported Pd nanoparticles. *Green. Chem.* **17**, 5009–5018 (2015).
- Cheng, J., Sulpizi, M., VandeVondele, J. & Sprik, M. Hole localization and thermochemistry of oxidative dehydrogenation of aqueous rutile TiO_2 (110). *ChemCatChem* **4**, 636–640 (2012).

35. Cheng, J., Liu, X., VandeVondele, J., Sulpizi, M. & Sprik, M. Redox potentials and acidity constants from density functional theory based molecular dynamics. *Acc. Chem. Res.* **47**, 3522–3529 (2014).
36. Cheng, J., Liu, X., Kattirtzi, J. A., VandeVondele, J. & Sprik, M. Aligning electronic and protonic energy levels of proton-coupled electron transfer in water oxidation on aqueous TiO₂. *Angew. Chem. Int. Ed.* **53**, 12046–12050 (2014).
37. Argyropoulos, S. D. et al. Quantitative ³¹P NMR detection of oxygen-centered and carbon-centered radical species. *Bioorg. Med. Chem.* **14**, 4017–4028 (2006).
38. Zoia, L. & Argyropoulos, S. D. Detection of ketyl radicals using ³¹P NMR spin trapping. *J. Phys. Org. Chem.* **23**, 505–512 (2010).
39. Müller, U., Rätzsch, M., Schwanninger, M., Steiner, M. & Zöbl, H. Yellowing and IR-changes of spruce wood as result of UV-irradiation. *J. Photochem. Photobiol. B* **69**, 97–105 (2003).
40. Fabbri, C., Bietti, M. & Lanzalunga, O. Generation and reactivity of ketyl radicals with lignin related structures. On the importance of the ketyl pathway in the photoyellowing of lignin containing pulps and papers. *J. Org. Chem.* **70**, 2720–2728 (2005).
41. Shuai, L. et al. Formaldehyde stabilization facilitates lignin monomer production during biomass depolymerization. *Science* **354**, 329–333 (2016).
42. Mansfield, S. D., Kim, H., Lu, F. & Ralph, J. Whole plant cell wall characterization using solution-state 2D NMR. *Nat. Protoc.* **7**, 1579–1589 (2012).
43. Wen, J., Sun, S., Xue, B. & Sun, C. Recent advances in characterization of lignin polymer by solution-state nuclear magnetic resonance (NMR) methodology. *Materials* **6**, 359–391 (2013).
44. VandeVondele, J. et al. Quickstep: fast and accurate density functional calculations using a mixed Gaussian and plane waves approach. *Comput. Phys. Commun.* **167**, 103–128 (2005).
45. Perdew, J. P., Burke, K. & Ernzerhof, M. Generalized gradient approximation made simple. *Phys. Rev. Lett.* **77**, 3865–3868 (1996).
46. Krukau, A. V., Vydrov, O. A., Izmaylov, A. F. & Scuseria, G. E. Influence of the exchange screening parameter on the performance of screened hybrid functionals. *J. Chem. Phys.* **125**, 224106 (2006).
47. Grimme, S., Antony, J., Ehrlich, S. & Krieg, H. A consistent and accurate ab initio parametrization of density functional dispersion correction (DFT-D) for the 94 elements H–Pu. *J. Chem. Phys.* **132**, 154104 (2010).
48. Frisch, M. J. et al. Gaussian 09 Revision D.01. (Gaussian, 2009).
49. Becke, A. D. Density-functional thermochemistry. 3. The role of exact exchange. *J. Chem. Phys.* **98**, 5648–5652 (1993).
50. Cossi, M., Rega, N., Scalmani, G. & Barone, V. Energies, structures, and electronic properties of molecules in solution with the C-PCM solvation model. *J. Comput. Chem.* **24**, 669–681 (2003).

Acknowledgements

This work was supported by the National Natural Science Foundation of China (Nos. 21690082, 91545203 and 21503176).

Author contributions

X.W. and X.F. performed most of the experiments and DFT computations, and analysed the data. S.X. performed some of the experiments and analysed the experimental data. J.L. performed characterizations for CdS QDs. J.C. guided the computational work, analysed all the data and co-wrote the paper. Q.Z. analysed all the data and co-wrote the paper. L.C. performed a part of characterizations and analysed the characterization results. Y.W. designed and guided the study and co-wrote the paper. All of the authors discussed the results and reviewed the manuscript.

Competing interests

The authors declare no competing interests.

Additional information

Supplementary information is available for this paper at <https://doi.org/10.1038/s41929-018-0148-8>.

Reprints and permissions information is available at www.nature.com/reprints.

Correspondence and requests for materials should be addressed to J.C. or Q.Z. or Y.W.

Publisher's note: Springer Nature remains neutral with regard to jurisdictional claims in published maps and institutional affiliations.